Robust Control of a Cable-Driven Soft Exoskeleton Joint for Intrinsic Human-Robot Interaction

C. Jarrett, *Student Member, IEEE*, and A. J. McDaid, *Member, IEEE*

***Abstract*— A novel, cable-driven soft joint is presented for use in robotic rehabilitation exoskeletons to provide intrinsic, comfortable human-robot interaction. The torque-displacement characteristics of the soft elastomeric core contained within the joint are modeled. This knowledge is used in conjunction with a dynamic system model to derive a sliding mode controller (SMC) to implement low-level torque control of the joint. The SMC controller is experimentally compared with a baseline feedback-linearised proportional-derivative controller across a range of conditions and shown to be robust to un-modeled disturbances. The torque controller is then tested with six healthy subjects while they perform a selection of activities of daily living, which has validated its range of performance. Finally, a case study with a participant with spastic cerebral palsy is presented to illustrate the potential of both the joint and controller to be used in a physiotherapy setting to assist clinical populations.**

***Index Terms*— Control engineering, rehabilitation robotics, series elastic actuator, sliding mode control, exoskeletons.**

I. Introduction

THE development of effective rehabilitation robotic systems presents many complex design and control challenges, which have been gathering much interest over recent years. Systems must be designed to impart high forces yet interact safely with patients who have limited physical and/or cognitive ability, be that with regards to strength, range of motion (ROM) or other neurological impairments. The major causes of such disability are stroke, spinal cord injury, traumatic brain injury and cerebral palsy (CP).

One major issue for robot design across all target populations is achieving inherent human-robot interaction (HRI). That is, how one is able to cooperate with a patient in a way that feels 'natural' and 'comfortable'. These performance characteristics are qualitative, subjective and can vary between and during tasks, hence are extremely difficult to design for.

HRI can be improved by incorporating features into the mechanical design of the device. One commonly used approach is to have passive degrees of freedom (DOF). Holley et al. built a device with 4DOF, of which only two are controlled [1]. A similar approach was taken by Gopura and Kiguchi where additionally, they attempted to incorporate a wide range of users by sizing their design based on 95th percentile anthropomorphic measurements [2].

Another interesting hardware approach is to use a series elastic actuator (SEA). An SEA is essentially a spring element placed in series with a stiff (and typically non-backdrivable) actuator to provide passive compliance. This technique has been widely used in literature [3]–[6].

Rehabilitation robotics control paradigms for HRI can be broadly split into low-level and high-level control. Within low-level control, the issues are well understood and there are large similarities between approaches. Many rehabilitation robots rely on impedance control [7] as a means of ensuring a natural interaction [4], [8], [9]; while a number of designs utilise admittance control [10], [11], with specific implementations depending on the environment and hardware.

HRI can be also improved through careful consideration of the high-level physiotherapy controllers. It has long been recognised that patient engagement is essential for effective rehabilitation [12]–[14], which has led to the "assist-as-needed" paradigm [15]–[19] and now error augmentation is receiving much attention [20]. Detecting user intent through electromyography (EMG) and electroencephalography (EEG) is also common in the design of human-robot rehabilitation systems. For example, Song et al. monitor EMG signals to determine when a patient cannot generate enough muscle force to move the device and assist them on the basis of this force [21]. However, such physiological signals are inherently complex and present many issues with regard to signal quality.

In general exoskeletons must be developed to be inherently safe, comfortable and robust. To this end, this paper presents a novel 'soft', compact and comfortable SEA design with an embedded biomechanical (kinematic and kinetic) sensor that is driven using Bowden cables from remote actuators. The control of the device is particularly challenging, given the large uncertainty in the system, which includes the unknown characteristics of each individual user. This problem is well recognised in current literature and other authors have suggested the use of robust control to overcome this uncertainty. Some research has focused on the application of techniques such as sliding mode control (SMC) and adaptive control for pure

Manuscript received March 23, 2016; revised October 25, 2016; accepted February 26, 2017. Date of publication March 1, 2017; date of current version August 6, 2017. This work was supported by Faculty of Engineering Research Development Fund, The University of Auckland.

The authors are with the Department of Mechanical Engineering, The University of Auckland, Auckland 1142, New Zealand (email: cjar160@aucklanduni.ac.nz; a.mcdaid@auckland.ac.nz).

Digital Object Identifier 10.1109/TNSRE.2017.2676765

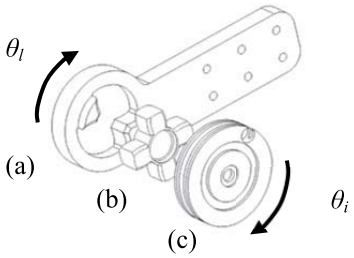

Fig. 1. The series elastic actuator with soft elastomer core. (a) Human output link, (b) elastomer coupling and (c) input driven by Bowden cables.

position tracking [22], [23]. Oxkul and Barkana [24] created an inner robust position controller based on a Kalman filter disturbance estimator, for use in an admittance controller. Miranda and Forner-Cordero used SMC and compared it in simulation to feedback linearisation with proportional control, for the purpose of creating a robust interaction force controller [25]. They found that SMC had superior performance characteristics to the feedback linearisation control, although this was in simulation. Furthermore, these devices did not use inherent, passive soft elements such as series elastic actuators in their actuator design.

With this in mind, a robust sliding mode controller (SMC) has been proposed as a low-level torque controller for the soft spring/damper-like joint. Its results are compared to a baseline feedback linearised proportional-derivative (PD) controller. An impedance controller is built on top of the torque controller. The system is implemented in a case study of an elbow exoskeleton where results are presented for six healthy subjects, as well as a case study with an adult participant with severe spastic CP. The performance in activities of daily living (ADLs) validates the system's potential as a rehabilitation/assistive device in clinical populations.

The main contribution of the paper is a new soft compact joint, driven by Bowden cables to enable a lightweight exoskeleton (with remote actuators) that contains inherent features aimed at increasing patient comfort and improving HRI. Both mechanical design and robust control have been considered in the implementation of the elbow case study; and this approach is transferable to other exoskeleton joints.

II. Bio-Joint & Sensor (BJS)

A. Configuration

A new robotic bio-joint and sensor (BJS) (Figure 1) has been designed to comfortably transfer torque to a soft biological joint, in this case a human. As shown in Figure 1, there are three main parts, (a) an output link connected directly to the limb to interact with the wearer, (b) an inner soft core manufactured using an elastomeric material and (c) an input joint, which is driven by Bowden cables from remote actuators (to physically offload the weight from the limb). θ_l and θ_i describe the rotation angles with respect to the transverse plane, of the output link and the input joint respectively. The torque is transferred from the inner joint through the elastomer, which allows the user to experience a degree of softness as they interact with the device. The elastomer has been geometrically designed based on Ruland torque couplings [26].

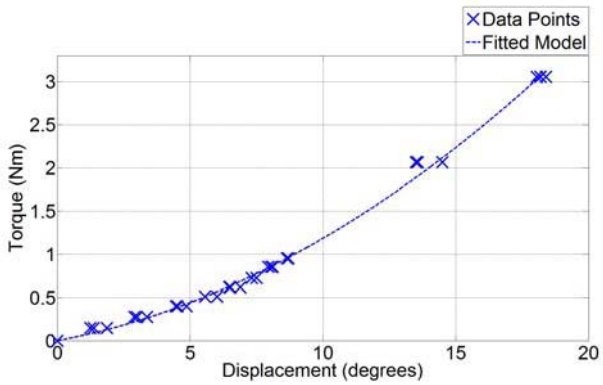

Fig. 2. Torque-displacement characteristics for the BJS.

θ_l and θ_i are measured directly using non-contact rotary Hall effect sensors which are integrated to make a compact assembly. The kinetic-kinematic characteristics of the spring element are controlled, which enables the human-robot torque on the limb to be directly calculated.

This new BJS configuration has advantages over traditional SEA configurations in that it has inherent damping so it feels more 'spongy' and hence comfortable than a spring where the restoring force (proportional to displacement) causes undesirable oscillatory characteristics for the wearer. On the other hand, these characteristics introduce issues which include inherent hysteresis and friction losses that can, for certain elastomer materials, become significant.

The elastomer core causes the torque-displacement relationship to be nonlinear, which provides a significant advantage when tailoring the characteristics to a user, since initially the interaction is "soft" to ensure comfort for small deviations (e.g. can absorb twitches and spasms) but then at higher forces becomes "stiffer" as necessary to transfer high torques (without large displacements). In addition the stiffness/damping characteristics can be easily altered by changing geometries and elastomer properties so they can be swapped between different participants; although obtaining a desired stiffness/damping characteristic for a given participant is a non-trivial modelling problem. The BJS is also very lightweight and compact so can reduce the overall size of the exoskeleton.

B. BJS Dynamics

As the required bandwidth for rehabilitation is relatively low [27] (<1Hz used in experiments) in comparison to the BJS natural frequency and the torque is typically varying slowly (i.e. $\dot{\theta}_l \approx \dot{\theta}_i$), the damping will not have a large influence. Based on pilot experiments the rate-independent hysteresis of the elastomer has been assumed negligible and the BJS torque-displacement characteristics assumed symmetric.

The measured torque-displacement characteristics for the loading case of a representative BJS joint are shown in Figure 2, and a second-order polynomial function was constructed to model the relationship, Equation 1, where $\Delta\theta$ refers to the relative displacement of the BJS components. It can be seen that this curve can be tailored to match a specific

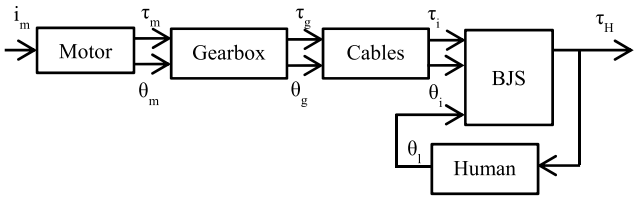

Fig. 3. Schematic of the robotic rehabilitation system.

desired interaction characteristic; in this study these specific characteristics were chosen because they allow a reasonable torque to be applied over a displacement suitable for the current geometry. Although humans are capable of producing larger torques, 3Nm was deemed adequate, given the ADLs performed in this study (Section VII).

$$\tau = \text{sgn}(\Delta\theta)0.0061\,(\Delta\theta)^2 + 0.0574\Delta\theta \tag{1}$$

III. System Modelling

Figure 3 illustrates the system architecture, assuming that a geared DC motor is driving the BJS, via cables attached to component c) from Figure 1. i_m is the motor current, τ_m is the torque exerted by the motor, τ_g is the torque exerted by the gearbox, τ_i is the torque exerted on the inner component of the BJS and τ_H is the human-robot interaction torque equivalent to that defined in Equation 1.

θ_m is the angle of the motor, θ_g is the angle of the gearbox, θ_i is the angle of the Bowden cable driven joint (Figure 1 (c)) and θ_l is the angle of the limb (Figure 1 (a)), which is equivalent to the angle of the outer BJS component.

Losses in the cables oppose the torque applied by the gearbox; $\tau_\text{i} = \tau_\text{g} - \tau_\text{c}$, where τ_c is the torque loss caused by the cables. However, the losses due to the cables are highly non-linear, time varying and dependent on highly uncertain factors, including cable tension and cable curvature. To simplify the modelling process, it was assumed that the dynamics of the cable are ideal. This has two implications. Firstly, $\theta_g = \theta_i$, and secondly, there can be assumed to be no torque loss in the cables, i.e. $\tau_c = 0$. The robust control method is used to compensate for this assumption, negating the need to develop an accurate friction model or observer, in addition to compensating for un-modelled elastomer dynamics. This is validated in the experimental results. A torque balance is taken about the inner joint, resulting in Equation 2:

$$\tau_g - \tau_H(\theta_i, \theta_l) = J_i\ddot{\theta}_i \tag{2}$$

where J_i is the effective inertia of the system as seen from the inner joint and $\tau_H(\theta_i,\theta_l)$ is the HRI torque generated in the BJS.

However, the gearbox is not ideal and losses occur due to friction. Thus a dynamic model of the gearbox and motor is required.

A. Modelling of the Motor and Gearbox

A two element friction model is used; comprising of coulomb and viscous components.

The gearbox dynamics under normal operation can thus be written as Equation 3, where n is the reduction ratio of the gearbox, b is the viscous damping coefficient and f_c is the coulomb friction coefficient of the motor.

$$\tau_g = n\tau_m - b\dot{\theta}_g - f_c sgn\left(\dot{\theta}_g\right) \tag{3}$$

Substituting into Equation 2 yields:

$$n\tau_m - b\dot{\theta}_g - f_c sgn(\dot{\theta}_g) - \tau_H(\theta_i, \theta_l) = J_i\ddot{\theta}_i \tag{4}$$

where $\theta_g = \theta_i$, so Equation 4 can be rewritten as:

$$n\tau_m - b\dot{\theta}_i - f_c sgn(\dot{\theta}_i) - \tau_H(\theta_i, \theta_l) = J_i\ddot{\theta}_i \tag{5}$$

IV. Robust Torque Controller

The structure of the BJS joint facilitates the implementation of a uniquely structured robust interaction torque controller, where the relative displacement between the two joint components dictates the torque on the joint.

There is a large degree of uncertainty associated with human-in-the-loop systems, due to difficulties in modelling, measuring and predicting human input, which is inherently variable. Furthermore, the BJS is cable driven, which introduces uncertainties due to variable friction losses. Friction losses are also present in the gearbox; in addition to non-linearities such as backlash. As such, an SMC controller [28] was implemented.

A. Derivation of Control Law

Let $\underline{\theta}$ represent the state vector. The tracking error, $\underline{\tilde{\theta}}$, can then be defined as Equation 6:

$$\underline{\tilde{\theta}} = \underline{\theta}_d - \underline{\theta} = [\tilde{\theta}_i, \dot{\tilde{\theta}}_i] \tag{6}$$

where $\underline{\theta}_d$ is the desired state vector.

A "sliding surface" is defined, which is a weighted sum of the tracking error.

$$s\left(\underline{\theta}, t\right) = \left(\frac{d}{dt} + \lambda\right)^{n-1}\tilde{\theta} \tag{7}$$

$$s\left(\underline{\theta}, t\right) = \dot{\tilde{\theta}} + \lambda\tilde{\theta} \tag{8}$$

where n is the order of the system and λ is a variable that describes the controller bandwidth.

The problem of tracking $\underline{\theta}$ can now be reduced to a first order stabilisation problem, namely keeping the value of s at 0. This can be achieved by fulfilling the following condition, known as the sliding condition, which is in reality Lyapunov's stability criterion.

$$\frac{1}{2}\frac{d}{dt}s^2 \leq \eta\,|s| \tag{9}$$

where η is chosen as an arbitrarily small constant.

To generate a control law to satisfy Equation 9, the dynamics of the sliding surface are first considered.

$$\dot{s} = (\ddot{\theta}_d - \ddot{\theta}_i) + \lambda(\dot{\theta}_d - \dot{\theta}_i) \tag{10}$$

Substituting dynamics from Equation 5 into Equation 10:

$$\dot{s} = (\ddot{\theta}_d - [\frac{1}{J_i}[n\tau_m - b\dot{\theta}_i - f_c sgn\left(\dot{\theta}_i\right) - \tau_H(\theta_i, \theta_l)]]) + \lambda(\dot{\theta}_d - \dot{\theta}_i) \quad (11)$$

Rearranging Equation 11 in terms of τ_m yields Equation 12, the "equivalent input", $\hat{\tau}_{eq}$, which keeps the sliding surface at 0 (if the parameters of the equation were perfectly known). Since the parameters are estimates, the variables are re-written with hat-notation in Equation 12.

$$\hat{\tau}_{eq} = \hat{J}_i\left[\ddot{\theta}_d + \lambda\left(\dot{\theta}_d - \dot{\theta}_i\right)\right] + b\dot{\theta}_i + f_c sgn\left(\dot{\theta}_i\right) + \hat{\tau}_H(\theta_i, \theta_l) \quad (12)$$

Furthermore, a compensatory term must be added to account for un-modelled dynamics. The complete control law is given by Equation 13.

$$u = \hat{\tau}_{eq} + k_{SMC} sgn\left(s\right) \quad (13)$$

To derive k_{SMC}, the system dynamics are substituted into Equation 9, now with the complete control law, to give Equation 14:

$$k_{SMC} \geq b_{unc}\dot{\theta}_i + f_{c_{unc}} sgn\left(\dot{\theta}_i\right) + \tau_{H_{unc}}(\theta_i, \theta_l) + J_i\eta + J_i[1-\beta][\ddot{\theta}_d + \lambda(\dot{\theta}_d - \dot{\theta}_i)] \quad (14)$$

where the subscript "unc" denotes the extent of uncertainty on variables, given by:

$$b_{unc}\dot{\theta}_i = b\dot{\theta}_i - \hat{b}\dot{\theta}_i \quad (15)$$

$$f_{c_{unc}} sgn\left(\dot{\theta}_i\right) = f_c sgn\left(\dot{\theta}_i\right) - \hat{f}_c sgn\left(\dot{\theta}_i\right) \quad (16)$$

$$\tau_{H_{unc}}(\theta_i, \theta_l) = \tau_{H_{unc}}(\theta_i, \theta_l) - \hat{\tau}_{H_{unc}}(\theta_i, \theta_l) \quad (17)$$

Selecting the uncertainty terms in Equations 15-17 is equivalent to specifying the upper and lower bounds of each estimated variable. Furthermore:

$$\beta \geq \frac{\hat{b}_{con}}{b_{con}} \quad (18)$$

where b_{con} is the control gain in the canonical form.

B. Controller Bandwidth and Chattering

λ is equivalent to the bandwidth of the controller, hence is extremely important in determining the system performance. Additionally, the nature of the compensatory term, k_{SMC}, is that it causes control chattering due to its switching nature. To address this problem, the term:

$$k_{SMC} sgn\left(s\right)$$

is replaced by:

$$k_{SMC} sat\left(\frac{s}{\phi}\right)$$

where *sgn* is the sign function and *sat* is the saturation function.

This causes the trajectory to converge to a boundary layer of width ϕ, rather than to the surface itself. This ensures smoother control, but at the expense of tracking performance.

Fig. 4. The mechanical structure of the rehabilitation device.

V. Elbow Exoskeleton Case Study

Thus far, the BJS and associated torque controller has been presented as a generalised system, capable of being applied to a range of joints. To validate the system experimentally, a case study was performed with an elbow exoskeleton device using the BJS component modeled in Figure 2. Figure 4 illustrates the device, which is designed taking into consideration anatomical properties and ergonomics for the elbow joint. It also contains a number of features aimed at improving the HRI.

A. Mechanical Design

A significant feature is the inclusion of passive joints. There is one active and three passive DOF in the design, illustrated in Figure 4. The first passive DOF (P1) is the steel rod; it is able to slide freely along its longitudinal axis due to the presence of linear bearings. It can also rotate about this axis, giving the second passive DOF (P2). The third passive DOF (P3) is found on the handle, which is able to rotate freely, allowing for wrist flexion and extension during exercises. The active degree of freedom controls elbow flexion and extension (A1).

These features are important because it means that the device can accommodate anatomical misalignments and changes in instantaneous center of rotation. This ensures that a patient does not have to locate their arm in a precise manner to use the device and if the exoskeleton moves during exercise, there are no adverse effects. This also allows a natural and comfortable fit for a large range of body sizes without adjustment. A secondary attachment has been created to allow for hands-free activities to be conducted as well. The weight of the device is kept low, less than 750g, since the actuators are remotely located.

A Maxon brushless direct current motor, with a maximum torque of 221mNm and a nominal speed of 3850rpm [29], is used with a reduction ratio of 74:1 [29]. There is a 1:1 connection between the gearbox and the elbow, thus the maximum speed of the forearm is 52rpm. A Maxon encoder was attached to the motor and used to measure its velocity. Attached to the gearbox is a set of Bowden cables which are connected to the exoskeleton BJS, specifically to the inner

TABLE I
ERRORS ON PARAMETRIC ESTIMATION

	Inertia (kgm^2)	Damping ($Nmsrad^{-1}$)	Coulomb Friction (Nm)	R^2 Values
Trial 1	0.1233	-0.1357	-0.0198	0.612
Trial 2	0.1661	-0.2003	-0.0284	0.672
Trial 3	0.1142	-0.1913	-0.2026	0.649
Average	**0.13**	**-0.18**	**-0.08**	**0.644**

component, illustrated in Figure 1. The purpose of the BJS in this exoskeleton is to actuate the elbow and is thus placed accordingly, beside the joint. As the motor turns, it moves the cables which rotate the BJS, thereby moving the forearm support and handle illustrated in Figure 4. This causes the elbow to flex and extend, with a ROM of 160°.

The position of the inner and outer BJS components were measured with the Hall effect rotary encoders. The velocities can be measured by applying a low-pass filter with 10 Hz cutoff frequency, based on experimental bandwidth testing, and a differentiating filter.

B. Calculation of Controller Variables

1) Estimation of System Parameters: To estimate J_i, b and f_c, an experiment similar to [30] was performed. Initially variables were taken from the datasheets [29] for the apparent inertia of the motor and gearbox, assumed to be $0.55kgm^2$, the viscous damping coefficient was assumed to be $0.5Nmsrad^{-1}$ and the coulomb friction was assumed to be 0.75Nm.

Once these parameters were applied, the gearbox was back-driven with the BJS attached to the end of the shaft to measure torque. Three trials were conducted and a least-squares linear regression in terms of torque, acceleration and velocity was performed.

The errors with respect to the initial estimations are depicted in Table 1. It is important to note that the recorded torque values rarely exceeded 1Nm, i.e. well within the range of the BJS model described in Section II-B.

When the initial compensation values are taken into account, the following estimates for the parameters of the specific motor are obtained.

- $J_i = 0.68\ kgm^2$
- $b = 0.32\ Nmsrad^{-1}$
- $f_c = 0.67\ Nm$

Note that J_i represents the apparent inertia of the entire system as seen from the inner component. The above estimate includes only the inertia provided by the motor and gearbox. However, excluding the human forearm, this is the primary source of inertia in the system. Furthermore, the following sections outline how it is possible to account for additional inertia with a robust controller design.

2) Remarks on Parameter Estimation by Linear Regression: The R^2 values are low, indicating a poorly fitted model. However, the purpose of this experiment was to obtain estimates of the parameters and thus precise values are not necessary. The uncertainty that this introduces lends further justification to the use of SMC as a control strategy.

C. Parametric Un-Certainty Estimation

The uncertainty terms in Equations 15-17 were selected as follows. For the viscous damping and coulomb friction coefficients, the uncertainty was chosen to be large; one and a half times the nominal value of damping and three times the nominal value of coulomb friction: $0.48Nmsrad^{-1}$ and 2Nm respectively.

The inertia uncertainty, required to correct the initial estimation of system inertia for Equation 12, was chosen to be $0.17kgm^2$. This is derived from an average forearm weight of 1.6kg and an average forearm length of 0.27m [31]. Using a slender rod approximation, this gives an estimated value of $0.117kgm^2$, with additional inertia added to account for variation between subjects.

The extent of uncertainty on the human-robot interaction torque was chosen in relation to the number of data points available for each section of the torque-displacement graph in Section III-C. At torques below 1Nm, the uncertainty was assumed to be 0.025Nm. At torques between 1Nm and 3Nm, it was assumed to be 0.25Nm.

D. Controller Bandwidth Selection

Through manual iterative tuning, it was found that a nominal value of $\lambda = 6$ gave an adequate balance between tracking performance and instability.

E. Selection of Boundary Layer Width

As mentioned, the nature of k_{SMC} causes the control input to chatter. This can be alleviated by careful selection of ϕ, the boundary layer width. In this research, ϕ was selected as 0.25. The difference in tracking error was on the order of 2 degrees and considered negligible.

VI. COMPARISON TO BASELINE CONTROLLER

To verify its ability to track a motion, the SMC controller was first compared in experiment to a baseline PD controller for pure trajectory tracking of the inner BJS component, i.e. tracking of θ_i. These experiments were performed without a human-in-the-loop, i.e. the exoskeleton brace was fixed in space, while the BJS components rotated, causing the exoskeleton handle to follow a desired trajectory. The setpoint for each experiment was chosen to be a variation of a sinusoidal chirp signal, as outlined below. In each case, the desired angle was compared to the actual angle as measured by the aforementioned rotary encoder built into the BJS.

The PD controller was supplemented with feedback linearisation terms equal to those modelled in the SMC controller: compensation for viscous friction, coulomb friction and inertia; in addition to the restoring torque of the BJS. In this manner, the following experiments determine the ability of SMC to account for un-modelled dynamics in comparison to a feedback-linearised PD controller.

Each controller was tested both for a range of trajectory profiles and in variable friction conditions; the latter achieved by intentionally twisting the cables, firstly with a 360° loop and secondly with a 720° loop.

The PD controller was tuned for an intermediate representative case, namely a sinusoid curve of 20° amplitude and 0.30Hz frequency. The gains were selected such that the trajectory converged to the setpoint on each oscillation without overshoot, representing an optimal response. This resulted in $K_p = 30\text{Nmrad}^{-1}$ and $K_d = 5\text{Nmsrad}^{-1}$.

A. Varying Amplitude

In the first set of experiments, small, medium and large amplitudes were chosen ranging from 0.01Hz to the upper frequency limit for that amplitude as dictated by hardware constraints: 10° amplitude to 0.7Hz, 20° amplitude to 0.6Hz and a large 40° amplitude to 0.4Hz. Figures 5a-5c are the frequency responses of the controller to these inputs. The nonlinearity (and potential instability in the PD case) of the system is evident by the variance of the bode plots at varying amplitudes.

In all testing scenarios, the PD controller has a low gain at low frequencies, indicating an inability to track the trajectory. It improves as the frequency increases and, when the amplitude was 10° and 20°, the gains caused overshoot at high frequencies, hence the positive magnitude response.

Conversely, the SMC has a far more consistent drop-off line, with almost no loss of gain in the 40° and 20° cases; and only dropping below -3dB at high frequencies of 0.63Hz in the 10° case. Furthermore, the SMC controller exhibits a lesser degree of phase difference in the 40° and 20° cases; and a less variable phase difference in the 10° case.

B. Varying Cable Friction

Figures 5d-5f show the frequency responses of the controllers for varying friction conditions in the Bowden cables, induced by changing the total cable bend angle. This is designed to show the robustness of the controller to unknown and varying parameters.

In the large majority of cases, the PD controller has a significantly lower gain response at low frequencies; this is due to the tuning of the controller, which is optimal in only one condition. At higher frequencies, it starts to overshoot the setpoint, resulting in gain values greater than 0dB.

For the case of 360° twist, the response was fairly similar to the case of no twist in the cables for both of the SMC and PD controllers. The PD controller begins with a low gain response and begins to overshoot at high frequencies; while the SMC controller has minimal drop-off.

The fact that the response of each controller has not significantly changed indicates that both were able to deal well with the disturbance. As expected, the steepest drop-off occurred in the case of highest friction; 720° twist. This was also the only condition that resulted in gain values lower than -3dB. There is a range of frequencies, from 0.3Hz to 0.5Hz, at which the PD controller is arguably outperforming the SMC controller for this test.

However, the gain response of the PD controller can be seen to be at -3dB for a larger range of frequencies (0.01-0.23Hz) in Figure 5f, compared to the SMC, which only dropped below -3dB at frequencies above 0.55Hz. Finally, it should be remembered that 720° represents an extreme case of friction, with two full loops of cable twist; severe conditions unlikely to be replicated in normal operation.

C. Remarks on Controller Performance

Overall, it is shown that the SMC controller has a superior frequency response to the PD controller, with higher magnitude responses at low frequencies and no tendency to overshoot at high frequencies; for the given gains. Across the large majority of the frequencies and amplitudes tested, the SMC controller was able to provide a satisfactory response, with the gain rarely dropping below -3dB.

On a qualitative basis, the SMC controller is preferred because, as expected, one set of gains has resulted in reasonably consistent performance, demonstrating its ability to be robust to a changing system. The response of the PD controller is far more variable whereas the compensatory term on the SMC controller has been able to adjust for both a range of trajectories and additional disturbances due to un-modelled friction. The PD controller could be improved by the use of gain-scheduling; however, this is out of the scope of this study.

VII. Human Participant Trials

Having validated the tracking ability and robustness of the SMC controller it was important to verify that it can fulfil its original purpose, to control HRI torque while a subject uses the device. To realise this control structure, Equations 19 and 20 were used to derive setpoints:

$$\theta_d = \theta_l + \theta_{offset} \tag{19}$$

$$\dot{\theta}_d = \dot{\theta}_l \tag{20}$$

where $\underline{\theta}_d$ represents the desired elbow dynamics and θ_{offset} is the desired relative displacement as derived from the torque-displacement relationship presented in Equation 1.

Three tests were then conducted on six healthy subjects performing ADLs; in addition to five tests on a subject with cerebral palsy. The testing was undertaken in accordance with the University of Auckland Human Participant Ethics Committee (UAHPEC) approval #010810.

A. Torque Controller Testing in ADLs

1) Experimental Procedure: The first (Task A) is derived from the Mayo Elbow Performance Index (MEPI), one part of which requires patients to "don a shirt" [32] and this task has been used elsewhere in rehabilitation research [33], [34]. Putting the shirt on was not practical with the current iteration of the exoskeleton, thus the task was modified to buttoning a shirt. Subjects were asked to begin from full elbow extension, before buttoning the shirt from top to bottom and ending with an extension. During the task, the exoskeleton was commanded to exert a force of 1Nm in the flexion direction.

The second (Task B) is derived from the Patient-Rated Tennis Elbow Evaluation [35] and requires that the patient drink from a glass of water. Other researchers have used variations of this task to evaluate patient ability [36]–[38] and

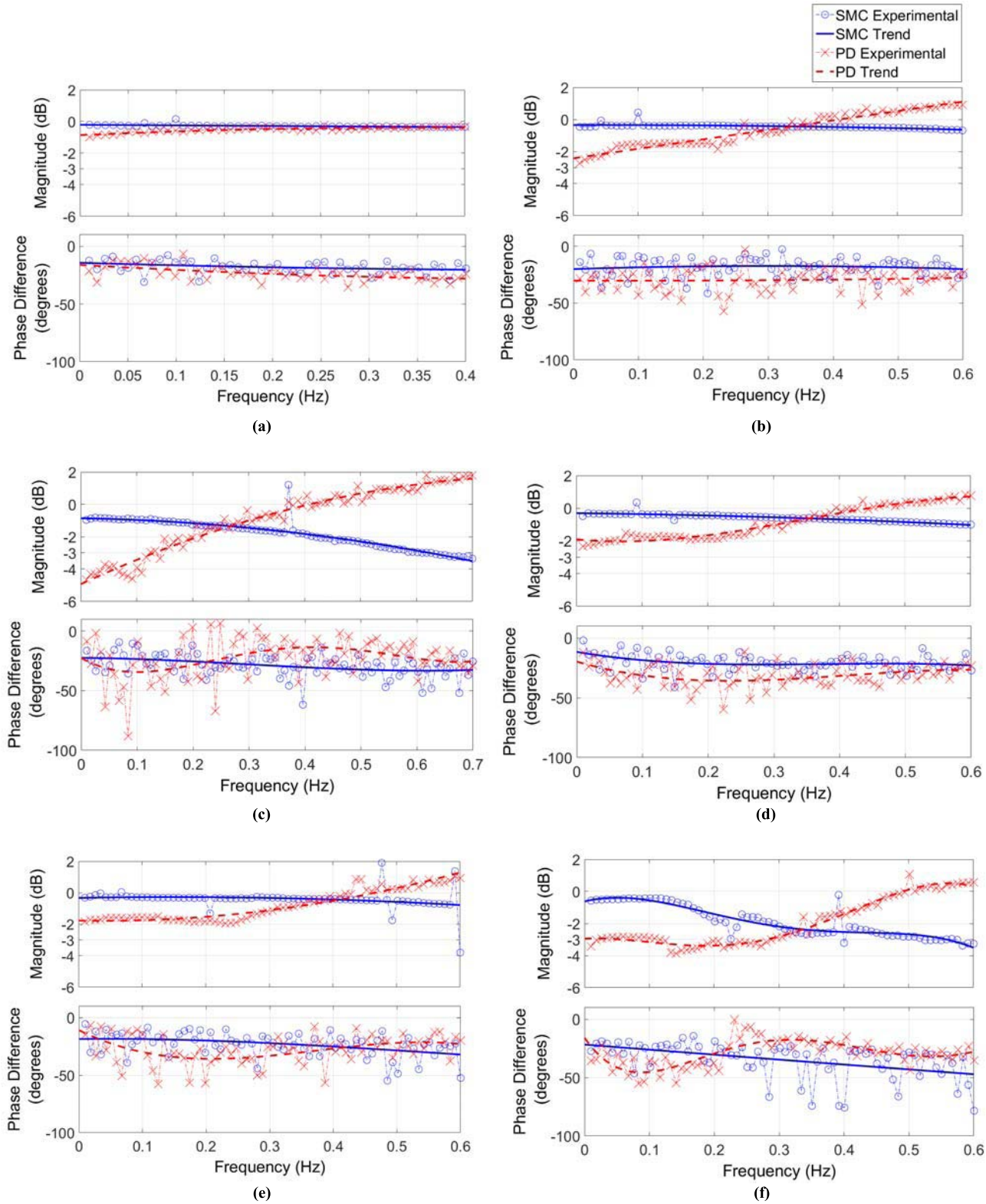

Fig. 5. Robustness testing of SMC and PD controllers (a) 40° input, (b) 20° input, (c) 10° input, (d) 20° input, 0° twist, (e) 20° input, 360° twist, (f) 20° input, 720° twist. Top: Magnitude response, bottom: phase response.

the final task was adapted from these variations and chosen to involve the user first pouring a glass of water and then drinking it. During the task, the exoskeleton was commanded to exert a torque of 1Nm in the extension direction.

2) Results: Table 2 displays the results of the first two ADLs performed by healthy subjects. Figure 6 displays a representative plot of each task, comparing the elbow angle measured by the Hall effect rotary encoder, to the

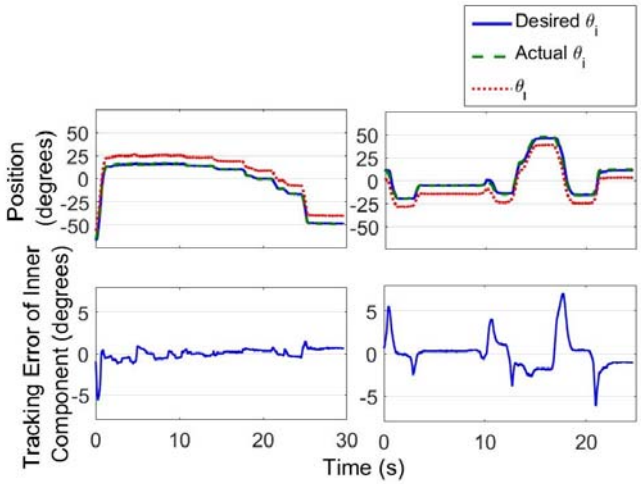

Fig. 6. Example response curves for BJS components during ADLs left: task a: buttoning a shirt, right: task b: drinking water. top: tracking performance, bottom: inner angle error plots.

TABLE II
RESULTS FOR HEALTHY PARTICIPANTS TORQUE TESTING

Subject	Task A RMS Error (deg)	Task B RMS Error (deg)
A	1.76	2.10
B	2.14	2.80
C	1.76	1.89
D	0.82	2.06
E	1.80	2.32
F	2.25	2.11
Average (SD)	1.76 (0.50)	2.21 (0.32)

desired angle. This illustrates the ability of the controller to accurately control the HRI torque by maintaining a constant offset between the inner and outer components of the BJS, despite unknown disturbances caused by interaction with human motion. It also exhibits the ability of the device and control system to support the motion needed during ADLs. The peaks in the error plots (bottom of Figure 6) arise due to sudden changes in motion, however in each case there is a fast decay to zero.

B. Impedance Control Testing

The impedance control test was designed to test the potential of the control system to be used in an impedance controller. Impedance control regulates a dynamic relationship between a desired position and torque to be applied to the arm. i.e. Equation 21, where J_d is the desired inertia, c_d is the desired damping and k_d is the desired stiffness.

$$\tau_d = J_d\ddot{\theta} + c_d\dot{\theta} + k_d\theta \tag{21}$$

In this research we chose to control the stiffness and damping so if a user deviates, the impedance control will act as a spring-damper, guiding them back to the path.

1) Experimental Procedure: During ADL Task A, the trajectory of the user was recorded. In the impedance control test, this trajectory was used as the set-point for the position of the elbow. The user was instructed to try to follow

TABLE III
RESULTS FOR TESTING IMPEDANCE CONTROL GAINS

	RMS Position Error (degrees)			HRI Torque (Nm)		
	Low	High	Decrease (%)	Low	High	Increase (%)
A	14.8	9.91	33.2	0.0805	0.107	13.0
B	6.93	5.48	21.0	0.160	0.117	-26.9
C	7.68	3.75	51.2	0.0920	0.0921	0.1
D	10.3	4.43	56.8	0.103	0.113	9.7
E	10.2	9.00	11.8	0.106	0.154	45.3
F	8.59	5.16	39.9	0.108	0.129	19.4
Average (SD)			35.7 (17.3)			13.4 (25.5)

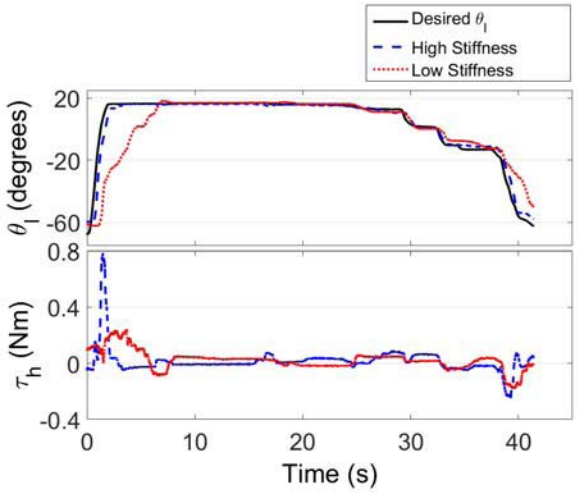

Fig. 7. Example plot response curve for impedance control testing top: tracking performance, bottom: HRI torque.

the trajectory as a graph presented on the computer screen. This task was performed twice, once with low impedance gains and once with high impedance gains. A nominal value of 0.25Nmrad^{-1} was selected for the stiffness and damping in the "low" case and a value of 0.75Nmsrad^{-1} was selected in the "high" case.

2) Results: Table 3 displays the RMS position error for each person that was tested, in addition to the RMS value for the torque that was applied to the elbow during the task. With high gains there was a 35.7% average decrease in RMS error. It was accompanied by a 10.1% average increase in the torque, suggesting that the improvement in tracking error was a result of the control algorithm and not the user's ability, with the exception of Subject B who had a change of -26.9%.

Figure 7 displays both a comparison of the observed motion for one subject and illustrates the second conclusion with the presence of larger peaks in measured torque in the high stiffness case. It can be seen also that in the case of the first peak, the torque applied by the BJS has reduced to 0 more quickly in the high gains case than the low gains case, indicating faster convergence to the trajectory.

The impedance test is important because it illustrates the ability of the BJS joint and control system to dynamically apply torques to the user's arm. It also illustrates the ability

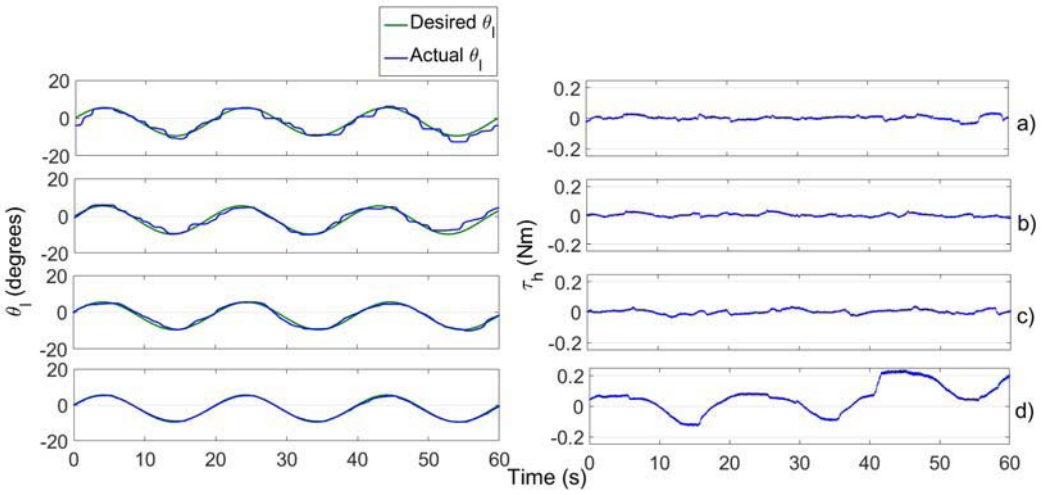

Fig. 8. Sample response for impedance testing with CP patient a) $k_d = 0$Nmrad^{-1}, $c_d = 0$Nmsrad^{-1} b) 0.25, 0.25, c) 0.75, 0.75 d) 20, 0.75. Left: Tracking Performance, Right: Measured HRI Torque.

of the system to help the user's joint track a trajectory, which is an important task in rehabilitation exercises.

C. Cerebral Palsy Participant Case Study

1) Experimental Procedure: A 43 year old male participant who has a diagnosis of CP (which has led to joint spasticity and limited ROM) and a self-reported score of IV on the MACS scale, was included in the study. He was first asked to extend and contract his arm as far as possible, to gauge his individual range of motion. A sinusoid trajectory was then offset to be centered on the mid-point of this range with amplitude equal to 75% of the patient's maximum ROM to ensure it could be reached and allow for overshoot if not properly controlled. Together, these constraints corresponded to a sinusoid that ranged from approximately $+6°$ to $-10°$.

A total of four trials were conducted with the participant to test the ability of the impedance controller. Initially, he was asked to attempt to follow a sinusoid of frequency 0.05Hz, with no assistance from the impedance controller. This was displayed to him with an on-screen graph. Following that, two further trials were conducted, where the gains of the impedance controller were chosen to match the gains selected for the experiments on able-bodied people. Finally, the stiffness was raised to 20Nmrad^{-1} and the damping was kept at 0.75Nmsrad^{-1}, i.e. essentially high gain position control of the elbow, to test the controller's capability.

2) Results: Table 4 displays the results for each trial performed by the cerebral palsy patient while tracking a 0.05 Hz trajectory. The table displays both RMS position error and the RMS torque measured at the BJS joint. The results are also displayed graphically in Figure 8.

It can be seen from Table 4 that as the gains of the impedance controller increase, the RMS position error decreases. Conversely, the BJS RMS torque increases, which is similar to the pattern observed in the tests on healthy subjects. It implies that the controller has acted to decrease the tracking error of the CP patient. There is one exception, namely that at gains of 0.25Nmrad^{-1} and 0.25Nmsrad^{-1}, the RMS HRI torque is less than the backdriven case. This suggests that the improvement in this case was due to the participant's own ability, which leads to a further conclusion that the gains were not high enough to influence the motion. As a final note, it can be observed that the HRI torque values are consistently lower than those of the healthy participants. This may be due to a number of reasons, including the slower motion used with the CP participant, the repetitive nature of a sine curve and the lack of the large step input observed in Figure 7, all of which contribute towards making the sine wave easier to follow than the ADL trajectory and thus requiring less assistive torque from the robot.

TABLE IV
RESULTS OF TESTING WITH CP PARTICIPANT

(k_d Nmrad^{-1})	(c_d Nmsrad^{-1})	RMS Position Error (degrees)	BJS RMS Torque (Nm)
0	0	1.80	0.0136
0.25	0.25	1.31	0.0108
0.75	0.75	0.942	0.0206
20.0	0.75	0.387	0.116

Figure 8 graphically illustrates the effect of increasing gains. It can be seen that with gains of 0.25, there is only a subtle visually observable improvement over the backdriven case, reinforcing the above conclusion that the gains were not strong enough to assist motion. However, in Figure 8c), the performance is markedly improved when compared to the backdriven response and at a stiffness of 20Nmrad^{-1}, the position tracking is almost perfect.

The results indicate the ability of the low-level SMC torque controller to be used as a part of a larger, multi-layered control structure. More specifically, it was able to generate torques that were sufficient to guide a cerebral palsy participant onto a desired trajectory; reducing the trajectory error of the participant.

3) Qualitative Patient Feedback: Following the trial with the device, the CP participant was asked a series of

questions pertaining to his experience using the device. He reported that it felt comfortable, that he could utilise his full ROM and that the straps on the device were comfortable. Furthermore, the patient believed that it would be possible to use his pointer to control his touch-screen computer while wearing the exoskeleton. With regards to the control of the device, the participant reported that it felt easier to follow the line as subsequent trials progressed, i.e. as the impedance gains were increased.

The feedback, overall, was positive and supports the use of the elbow device, soft joint and control system for further development and testing.

VIII. Conclusions and Future Work

In this study, SMC has been investigated as a means of controlling a novel series elastic actuator, known as a compliant Bio-Joint & Sensor (BJS). The new joint has a number of advantages over current SEA configurations and the method of control, SMC, has been shown to be more robust to un-modelled disturbances than a feedback-linearised PD controller and that it can adapt to follow a variety of trajectories.

The SMC controller has also been shown to generate sufficient control action and have sufficient bandwidth to enable a user to perform a selection of ADLs, in addition to proving that it can be used in a multi-layered control structure to assist a cerebral palsy participant in reducing tracking error for a sinusoidal trajectory. These results suggest its potential to be used as an inner torque controller for more complex rehabilitation paradigms.

In future work, the authors will investigate the use of different materials in the construction of the BJS joint; to enable a larger range of torque sensing and actuation to be realised. Additional high-level torque controllers will be developed and the use of the inner SMC torque controller in these control paradigms will be investigated. Finally, the authors wish to implement the joint structure on more rehabilitation systems, focusing on more complex joints with multiple DOFs.

Acknowledgments

Special thanks also to Vinura Jayaneththi and John-Zaymon Viloria, who completed the mechanical design of the exoskeleton used as a case study.

References

[1] D. Holley, M. Johnson, G. Harris, and S. Beardsley, "A modular low-clearance wrist orthosis for improving wrist motion in children with cerebral palsy," in *Proc. 36th Annu. Int. Conf. IEEE Eng. Med. Biol. Soc. (EMBC)*, Aug. 2014, pp. 3069–3072.

[2] R. A. R. C. Gopura and K. Kiguchi, "EMG-based control of an exoskeleton robot for human forearm and wrist motion assist," in *Proc. IEEE Int. Conf. Robot. Autom. (ICRA)*, May 2008, pp. 731–736.

[3] J. F. Veneman, R. Kruidhof, E. E. G. Hekman, R. Ekkelenkamp, E. H. F. V. Asseldonk, and H. V. D. Kooij, "Design and evaluation of the LOPES exoskeleton robot for interactive gait rehabilitation," *IEEE Trans. Neural Syst. Rehabil. Eng.*, vol. 15, no. 3, pp. 379–386, Sep. 2007.

[4] K. Kong, J. Bae, and M. Tomizuka, "A cable-driven human assistive system and its impedance compensation by sensor fusion," in *Proc. ASME Dyn. Syst. Control Conf.*, Jan. 2010, pp. 835–842.

[5] V. R. Ham and T. G. Sugar, "Adjustable robotic tendon using a 'Jack Spring,'" in *Proc. IEEE 9th Int. Conf. Rehabil. Robot.*, Jul. 2005, pp. 113–118.

[6] J. Oblak, I. Cikajlo, and Z. Matjacic, "A universal haptic device for arm and wrist rehabilitation," in *Proc. IEEE Int. Conf. Rehabil. Robot.*, Jun. 2009, pp. 436–441.

[7] N. Hogan, "Impedance control: An approach to manipulation: Part II—Implementation," *J. Dyn. Syst., Meas., Control*, vol. 107, no. 1, pp. 8–16, 1985.

[8] Y. H. Tsoi and S. Q. Xie, "Impedance control of ankle rehabilitation robot," in *Proc. IEEE Int. Conf. Robot. Biomimetics (ROBIO)*, Feb. 2009, pp. 840–845.

[9] A. Denève, S. Moughamir, L. Afilal, and J. Zaytoon, "Control system design of a 3-DOF upper limbs rehabilitation robot," *Comput. Methods Programs Biomed.*, vol. 89, pp. 202–214, Feb. 2008.

[10] R. Colombo *et al.*, "Robotic techniques for upper limb evaluation and rehabilitation of stroke patients," *IEEE Trans. Neural Syst. Rehabil. Eng.*, vol. 13, no. 3, pp. 311–324, Sep. 2005.

[11] Y. Yang, L. Wang, J. Tong, and L. Zhang, "Arm rehabilitation robot impedance control and experimentation," in *Proc. IEEE Int. Conf. Robot. Biomimetics (ROBIO)*, Dec. 2006, pp. 914–918.

[12] N. F. Skinner, "Learned Helplessness: Performance as a function of task significance," *J. Psychol.*, vol. 102, no. 1, pp. 77–82, 1979.

[13] S. Jezernik, R. Schärer, G. Colombo, and M. Morari, "Adaptive robotic rehabilitation of locomotion: A clinical study in spinally injured individuals," *Spinal Cord*, vol. 41, pp. 657–666, Dec. 2003.

[14] R. A. Schmidt and R. A. Bjork, "New conceptualizations of practice: Common principles in three paradigms suggest new concepts for training," *Psychol. Sci.*, vol. 3, no. 4, pp. 207–217, 1992.

[15] D. Erol and N. Sarkar, "Design and implementation of an assistive controller for rehabilitation robotic systems," *Int. J. Adv. Robot. Syst.*, vol. 4, pp. 271–278, Sep. 2007.

[16] D. Erol and N. Sarkar, "Intelligent control for robotic rehabilitation after stroke," *J. Intell. Robot. Syst.*, vol. 50, no. 4, pp. 341–360, 2007.

[17] J. L. Emken, J. E. Bobrow, and D. J. Reinkensmeyer, "Robotic movement training as an optimization problem: Designing a controller that assists only as needed," in *Proc. IEEE 9th Int. Conf. Rehabil. Robot.*, Jul. 2005, pp. 307–312.

[18] L. Marchal-Crespo and D. J. Reinkensmeyer, "Review of control strategies for robotic movement training after neurologic injury," *J. NeuroEng. Rehabil.*, vol. 6, p. 20, Jun. 2009.

[19] U. Keller, G. Rauter, and R. Riener, "Assist-as-needed path control for the PASCAL rehabilitation robot," in *Proc. IEEE Int. Conf. Rehabil. Robot. (ICORR)*, Jun. 2013, pp. 1–7.

[20] F. Abdollah *et al.*, "Error augmentation enhancing arm recovery in individuals with chronic stroke: A randomized crossover design," *Neurorehabilitation Neural Repair*, vol. 28, pp. 120–128, Feb. 2014.

[21] R. Song, K. Tong, X. Hu, and W. Zhou, "Myoelectrically controlled wrist robot for stroke rehabilitation," *J. Neuroeng. Rehabil.*, vol. 10, p. 52, Jun. 2013.

[22] H. B. Kang and J. H. Wang, "Adaptive robust control of 5 DOF upper-limb exoskeleton robot," *Int. J. Control, Autom., Syst.*, vol. 13, no. 3, pp. 1–9, 2015.

[23] A. Wege, K. Kondak, and G. Hommel, "Mechanical design and motion control of a hand exoskeleton for rehabilitation," in *Proc. Int. Conf. Mechatronics Autom. (ICMA)*, Niagara Falls, Canada, Aug. 2005, pp. 155–159.

[24] F. Ozkul and D. E. Barkana, "Design of an admittance control with inner robust position control for a robot-assisted rehabilitation system RehabRoby," presented at the IEEE/ASME Int. Conf. Adv. Intell. Mechatronics (AIM), Budapest, Hungary, Jul. 2011, pp. 104–109.

[25] A. B. W. Miranda and A. Forner-Cordero, "Upper limb exoskeleton control based on sliding mode control and feedback linearization," presented at the Biosignals Biorobotics Conf. (ISSNIP), Rio de Janeiro, Brazil, Feb. 2013, pp. 1–6.

[26] Ruland. (2015). *Jaw Coupling Spiders*. [Online]. Available: http://www.ruland.com/ps_couplings_jaw_spider.asp

[27] M. Lamotte, F. Fleury, M. Pirard, A. Jamon, and P. van de Borne, "Acute cardiovascular response to resistance training during cardiac rehabilitation: Effect of repetition speed and rest periods," *Eur. J. Cardiovascular Prevention Rehabil.*, vol. 17, pp. 329–336, Jan. 2010.

[28] J. E. Slotine and W. Li, *Applied Nonlinear Control*. Englewood Cliffs, NJ, USA: Prentice-Hall, 1991.

[29] Maxon Motors, *Program 2013/14: High Precision Drives and Systems*. 2013, pp. 224–274. [Online]. Available: https://www.scribd.com/document/245997778/MAXON-Catalog-2013-2014

[30] N. L. Tagliamonte, D. Formica, M. Scorcia, D. Campolo, and E. Guglielmelli, "Force control of a robot for wrist rehabilitation: Towards coping with human intrinsic constraints," in *Proc. IEEE/RSJ Int. Conf. Intell. Robots Syst. (IROS)*, Oct. 2010, pp. 4384–4389.

[31] S. Plagenhoef, F. G. Evans, and T. Abdelnour, "Anatomical data for analyzing human motion," *J. Res. Quart. Exercise Sport*, vol. 4, no. 2, pp. 169–178, 1983.

[32] B. F. Morrey and R. A. Adams, "Semiconstrained arthoplasty for the treatment of rheumatoid arthtritis of the elbow," *Joint Replacement Arthoplasty*, vol. 74, pp. 479–490, Apr. 1992.

[33] Y. G. Rhee, N. S. Cho, C. T. Lim, and J. W. Yi, "Debridement arthroplasty for post-traumatic stiff elbow: Intraoperative factors affecting the clinical results of surgical treatment," *Clin. Orthopedic Surgery*, vol. 1, pp. 27–33, Mar. 2009.

[34] D. R. Gill and B. F. Morrey, "The Coonrad-Morrey total elbow arthroplasty in patients who have rheumatoid arthritis. A ten to fifteen-year follow-up study," *J. Bone Joint Surgery Amer.*, vol. 80, pp. 1327–1335, Sep. 1998.

[35] J. C. M. Dermid, "The patient-rated tennis elbow evaluation (PRTEE) user manual," Clin. Res. Lab, Hand Upper Limb Centre School Rehabil. Sci., McMaster Univ., Hamilton, ON, Canada, Tech. Rep., 2007.

[36] B. V. Somanchi and L. Funk, "Evaluation of functional outcome and patient satisfaction after arthroscopic elbow arthrolysis," *Acta Orthopaedica Belgica*, vol. 74, no. 1, pp. 17–23, 2008.

[37] M. Sardelli, R. Z. Tashjian, and B. A. MacWilliams, "Functional elbow range of motion for contemporary tasks," *J. Bone Joint Surgery*, vol. 93, pp. 471–477, Mar. 2011.

[38] P. Raiss, O. Rettig, S. Wolf, M. Loew, and P. Kasten, "Range of motion of shoulder and elbow in activities of daily life in 3D motion analysis," *Zeitschrift fur Orthopadie und Unfallchirurgie*, vol. 145, pp. 493–498, Jul. 2007.